The optimizing of thickness combination in organic solar cells with the concept of effective exciton generation rate

XI XI[a,b,c], XIAOJING CHEN[b,c], YING GUO[a,c], GUOHUA LI[a,c,*]
[a]*School of Science, Jiangnan University, 1800 Lihu Ave., Wuxi, China, 214122*
[b]*Wuxi Suntech Power Co., Ltd., 12 Xinhua Road, Wuxi, China, 214028*
[c]*Jiangsu Optoelectronic Engineering and Technology Research Cente, 1800 Lihu Ave., Wuxi, China, 214122*

Organic Solar Cells are attracting a great deal of attention now. However, the academic system of organic solar cells is still not so perfect. Most of the active layers' thickness combinations are carried out from practical experiments. The theoretic process for this subject is still unsubstantial. In this paper, a concept of effective exciton generation rate, based on light intensity distribution, is given. For maximizing this rate, the thickness combination of active layers can be obtained. In order to keep the simulation process closer to practical fabrication, photon flux distribution of AM1.5G and transmisstivity of substrates were introduced into the calculation. Although there an error of a few nanometers exists between the results of simulation and experiments, it is in an acceptable range. The reason of this error has also been analyzed. The main contribution of this method is that it gives a search range of thickness combination of donor and acceptor layers.

(Received February 11, 2014; accepted May 7, 2015)

Keywords: Organic Solar Cells, Effective Exciton, Generation Rate, Thickness Combination

1. Introduction

Organic solar cells (OSCs) are attracting a great deal of attention, because of flexibility, low cost, light weight and large-area application [1-11]. From the first double-structured solar cell introduced by Tang [12], different methods have been proposed in order to improve the power conversion efficiency and the stability of organic solar cells. The mechanisms can be roughly concluded into three processes [13]: 1) generation of excitons; 2) exciton dissociation; 3) carrier collection. Many efforts have been made to improve the efficiency, such as modification of electrodes, development of new structures. More and more researchers put their emphasis on experiments. However the academic system of organic solar cells is not so perfect now. Many problems are still not so clear in theory, for example, the thickness combination of active layers. Most data of these combinations come from practical experiments. Although qualitative analysis is usually given after these experiments, theoretical process for the criterion of optimal active material thickness combination is still unsubstantial. In this paper, the optimizing of thickness combination starts from the generation of excitons. A concept of effective exciton generation rate is established. The optimal thickness combination will be obtained by maximizing this rate.

2. Modeling

The average energy flux density "*S*" of a beam light at a unit area is proportional to its intensity (*I*) [14],

$$S = \frac{n\varepsilon_0 c}{2} I \tag{1}$$

where ε_0 and c are the dielectric constant and light rate in vacuum, respectively; n is the refractive index of the material; $I = \left|\tilde{E}\right|^2$ ($\tilde{E}$ is the electric field of the light).

When a beam of light with an average energy flux density S irradiates intro a material, the average absorption power at a unit area can be described as follow [14],

$$Q = \frac{2\pi}{\lambda}\kappa S = \frac{\pi\varepsilon_0 c\kappa n}{\lambda} I \tag{2}$$

where λ is the wavelength of the light; κ is the extinction coefficient of the material.

Thus the number of absorption photons at a unit area per second is

$$P = \frac{Q}{hc/\lambda} = \frac{\pi\varepsilon_0 \kappa n}{h} I \tag{3}$$

where h is the Planck constant.

Let $C = \frac{\pi\varepsilon_0}{h}$, then

$$P = C\kappa nI \tag{4}$$

Assuming that all these photons can be used to produce excitons and thus its efficiency is 100% [13]. The number of photon-generated excitons at a unit area per second equals to *P*,

$$g = P = C\kappa nI \tag{5}$$

Eq.(5) is the exciton generation rate at a unit area.

g is related to the intensity (*I*), and the materials (κ, *n*), while *I* is a function of the position inside devices. Additionally, it is necessary to point out what the wavelength is and at which layer the excitons generate. So Eq. (5) can be rewritten as

$$g_{\lambda,j}(x) = C\kappa_{\lambda,j} n_{\lambda,j} \left|\tilde{E}_{\lambda,j}(x)\right|^2 \tag{6}$$

$g_{\lambda,j}(x)$ represents exciton generation rate at the position *x* at a unit area, inside the material *j*, after absorbing the light with the wavelength of λ.

Of course, this equation is only suitable for active materials, otherwise $g_{\lambda,j}(x) \equiv 0$

The actual sunlight energy, as well as the photon flux density, is not a uniform distribution over wavelengths. Additionally, the substrate, usually glass is used, does not show a uniform transmissivity either. So far, an actual effect of $g_{\lambda,j}(x)$ needs to be improved to

$$g_{\lambda,j}(x) = C\Phi_\lambda T_\lambda \kappa_{\lambda,j} n_{\lambda,j} \left|\tilde{E}_{\lambda,j}(x)\right|^2 \tag{7}$$

where Φ_λ is the photon flux density of AM1.5G at wavelength λ, and T_λ is the transmissivity of substrates at this wavelength.

Thus, for the response wavelength range ($[\lambda_1, \lambda_2]$) of the device, the total exciton generation rate can be described as

$$g_j(x) = \int_{\lambda_1}^{\lambda_2} g_{\lambda,j}(x)d\lambda = \int_{\lambda_1}^{\lambda_2} C\Phi_\lambda T_\lambda \kappa_{\lambda,j} n_{\lambda,j} \left|\tilde{E}_{\lambda,j}(x)\right|^2 d\lambda \tag{8}$$

Not all the excitons can be dissociated into electrons and holes. Only excitons which are very near the donor/acceptor (D/A) interface can be separated. These excitons are called effective excitons. And this range is within an exciton diffusion length inside donor and acceptor layers near the D/A interface, respectively. So the effective exciton generation rate will be

$$G = \int_{x_{D/A}-\min[d_D,L_D]}^{x_{D/A}+\min[d_A,L_A]} \left[\int_{\lambda_1}^{\lambda_2} C\Phi_\lambda T_\lambda \kappa_{\lambda,j} n_{\lambda,j} \left|\tilde{E}_{\lambda,j}(x)\right|^2 d\lambda\right] dx \tag{9}$$

Here assuming that sunlight transfers through the donor layer firstly in cell structure. $x_{D/A}$ is the position of D/A interface. d_A, d_D are the thicknesses of donor and acceptor layers, respectively. L_D and L_A are the exciton diffusion lengths in donor and acceptor layers, respectively.

In Eq. (9), the effective exciton generation rate is surely related to the light intensity distribution ($\left|\tilde{E}_{\lambda,j}(x)\right|^2$) inside cells. Here, this rate is additionally related to incident light and materials. $\Phi_\lambda T_\lambda$ characterizes the photon flux density distribution in active materials; and $\kappa_{\lambda,j}$ characterizes the absorption spectrum of material *j*. The summation of generation rate in effective spaces and response wavelength range are adequately considered by the integrals of position and wavelength. So Eq. (9) exhibits more information of exciton generation and explains the generation process of effective excitons further.

In Eq. (9) there are four different cases,

1° $d_D \geq L_D$, $d_A \geq L_A$,

$$G = \int_{x_{D/A}-L_D}^{x_{D/A}+L_A} g_j(x)dx = \int_{x_{D/A}-L_D}^{x_{D/A}+L_A} \left[\int_{\lambda_1}^{\lambda_2} C\Phi_\lambda T_\lambda \kappa_{\lambda,j} n_{\lambda,j} \left|\tilde{E}_{\lambda,j}(x)\right|^2 d\lambda\right] dx$$

2° $d_D < L_D$, $d_A \geq L_A$,

$$G = \int_{x_{D/A}-d_D}^{x_{D/A}+L_A} g_j(x)dx = \int_{x_{D/A}-d_D}^{x_{D/A}+L_A} \left[\int_{\lambda_1}^{\lambda_2} C\Phi_\lambda T_\lambda \kappa_{\lambda,j} n_{\lambda,j} \left|\tilde{E}_{\lambda,j}(x)\right|^2 d\lambda\right] dx$$

3° $d_D \geq L_D$, $d_A < L_A$,

$$G = \int_{x_{D/A}-L_D}^{x_{D/A}+d_A} g_j(x)dx = \int_{x_{D/A}-L_D}^{x_{D/A}+d_A} \left[\int_{\lambda_1}^{\lambda_2} C\Phi_\lambda T_\lambda \kappa_{\lambda,j} n_{\lambda,j} \left|\tilde{E}_{\lambda,j}(x)\right|^2 d\lambda\right] dx$$

4° $d_D < L_D$, $d_A < L_A$,

$$G = \int_{x_{D/A}-d_D}^{x_{D/A}+d_A} g_j(x)dx = \int_{x_{D/A}-d_D}^{x_{D/A}+d_A} \left[\int_{\lambda_1}^{\lambda_2} C\Phi_\lambda T_\lambda \kappa_{\lambda,j} n_{\lambda,j} \left|\tilde{E}_{\lambda,j}(x)\right|^2 d\lambda\right] dx$$

Effective exciton generation rate is related to the thickness combination of donor and acceptor layers. The larger this rate is, the better cell performances will exhibit. So from Eq.(9) maximizing *G*, the optimal thickness combination can be obtained.

3. Results and discussion

The concept of effective exciton generation rate is based on light intensity distribution inside cells. Many methods can be used to calculate light intensity. The calculation process of light intensity distribution is not the emphasis in this paper. Here the theory of optical transmission matrix is applied.

Organic solar cells can be seen as an optical stack formed by several ultrathin films. The matrices are preciously applied to organic solar cells by Pettersom et al. [15]. Homogeneous and isotropic materials are assumed and described by complex index of refraction, $\hat{n}$, where $\hat{n} = n - i \cdot \kappa$. n is refraction index and κ is extinction coefficient of materials. Furthermore, the interfaces are assumed to be optically flat. The optical electric field amplitude *E(x)* is calculated as a function of position in the multilayer structure, where $E(x) = \begin{bmatrix} E^+(x) \\ E^-(x) \end{bmatrix}$. $E^+(x)$ and $E^-(x)$ are the components of the optical electric field propagating in the positive and the negative directions.

At an interface between layer *j* and *k* (see Fig. 1), the transmission of the optical field is described by the interface matrix T_{jk} as

$$\begin{bmatrix} E_j^+ \\ E_j^- \end{bmatrix} = T_{jk} \begin{bmatrix} E_k^+ \\ E_k^- \end{bmatrix} \tag{10}$$

where $T_{jk} = \frac{1}{t_{jk}} \begin{bmatrix} 1 & r_{jk} \\ r_{jk} & 1 \end{bmatrix}$, $t_{jk} = \frac{2\hat{n}_j}{\hat{n}_j + \hat{n}_k}$,

$r_{jk} = \frac{\hat{n}_j - \hat{n}_j}{\hat{n}_j + \hat{n}_k}$

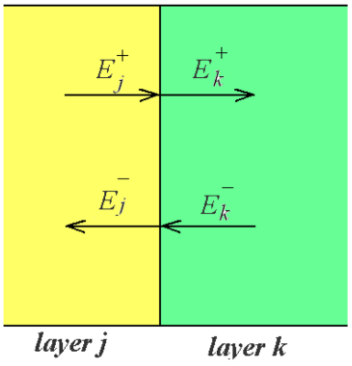

Fig. 1. Sketch of the optical transmission at the interface of two thin films.

The transmission through a layer *m* (see Fig. 2) can be described as

$$\begin{bmatrix} E_{m0}^+ \\ E_{m0}^- \end{bmatrix} = L_m \begin{bmatrix} E_{mn}^+ \\ E_{mn}^- \end{bmatrix} \tag{11}$$

where $L_m = \begin{bmatrix} \exp\left(\frac{2\pi i \hat{n}_m d_m}{\lambda}\right) & 0 \\ 0 & \exp\left(-\frac{2\pi i \hat{n}_m d_m}{\lambda}\right) \end{bmatrix}$, d_m is this layer's thickness, λ is the wavelength of the light.

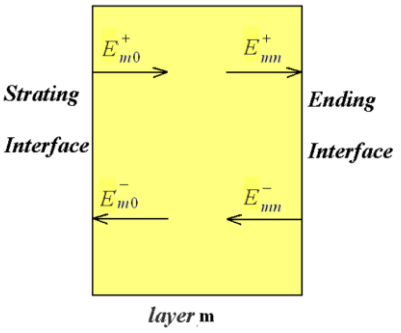

Fig. 2. Sketch of the optical transmission inside a single thin film.

Thus the transmission inside the following stack is shown in Fig. 3.

Then

$$E_0(0) = \left\{ T_{01} \prod_{j=1}^{m} \left[L_j T_{j(j+1)} \right] \right\} \cdot E_m(x_{m-1}) \tag{12}$$

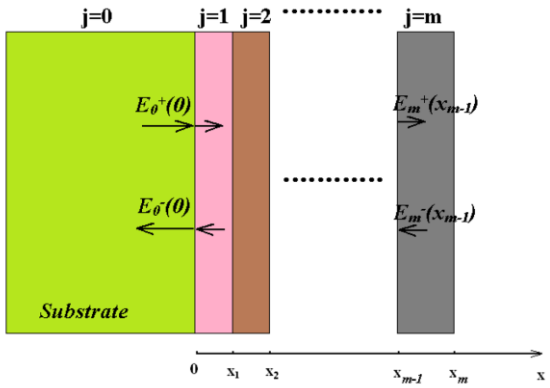

Fig. 3. The light propagation model inside a multi-layer device.

Since substrates are usually much thicker than other layers, the optical interference effect is not applicable.

The total electric field at arbitrary position inside layer *j* is given in terms of the electric field of the incident wave by

$$\tilde{E}_j(x) = E_j^+(x) + E_j^-(x) = \exp\left(-\frac{2\pi i \hat{n}_j (x - x_{j-1})}{\lambda}\right) E_j^+(x_{j-1}) + \exp\left(\frac{2\pi i \hat{n}_j (x - x_{j-1})}{\lambda}\right) E_j^-(x_{j-1}) \quad (13)$$

where x_{j-1} is the position of starting interface in layer *j*.

Light intensity distribution inside devices can be obtained from Eq. (10) ~ Eq. (13). Introducing intensity distribution function into Eq. (9), effective exciton generation rate can be calculated.

Here, a small molecule organic solar cell is used as an example to calculate its effective exciton generation rate. Since the better performance of C_{70} [16] and PEDOT:PSS/LiF anode buffer layer system [17], Glass/ITO(220 nm)/PEDOT:PSS(40 nm)/LiF(1 nm)/CuPc/C_{70}/LiF(1 nm)/Al(100 nm) is used as the cell's structure. The response range of the cell is from the wavelength of 300 nm to 800 nm [16]. The refractive indexes and extinction coefficients of the materials measured by a full spectrum ellipsometer in this range are shown in Fig. 4.

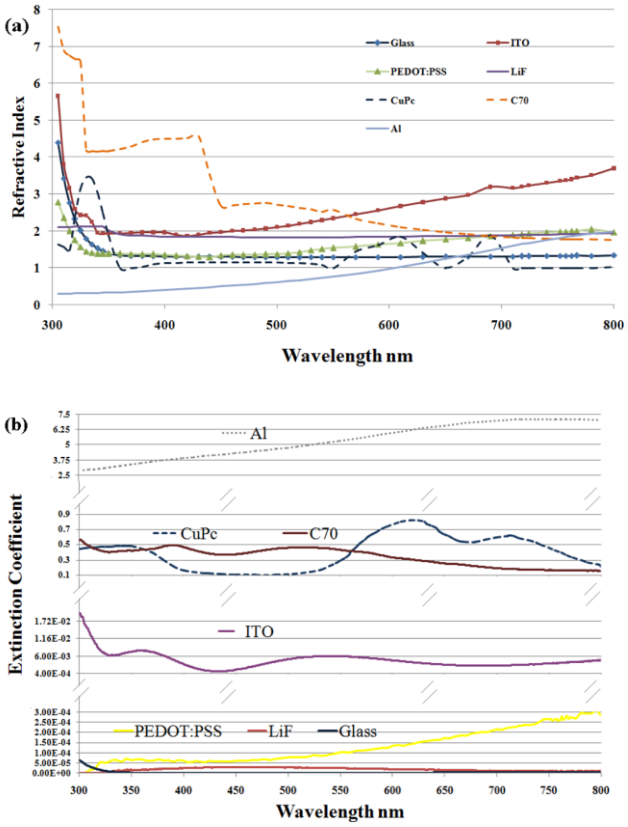

Fig. 4. Complex refractive indices of the materials (a) refractive indices, (b) extinction coefficients.

The transmissivity spectrum of the glass substrate and the photon flux density of AM1.5G are also shown in Fig. 5, where Φ_λ is a relative value. The photon flux density at each wavelength in Fig. 5 is related to the one at 550 nm, the data is 4.3243×10^{14} $((cm^2s)^{-1})$ from "IEC 60904–3: 2008, ASTM G-173-03 global".

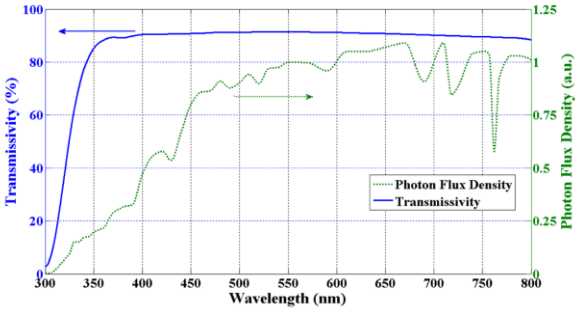

Fig. 5. The transmissivity spectrum of the glass substrate and the photon flux density of AM1.5G. The photon flux density at each wavelength is related to the one at 550 nm, the data is 4.3243×10^{14} $((cm^2s)^{-1})$ from "IEC 60904–3: 2008, ASTM G-173-03 global".

The effective exciton generation rate of this cell was calculated. The relationship between this rate, thicknesses of CuPc and C_{70} is shown in Fig. 6.

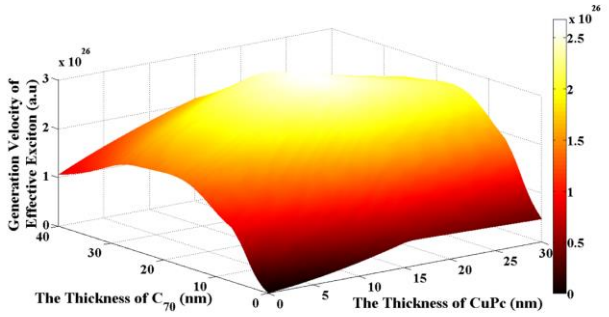

Fig. 6. The relation between generation rate of effective excitons, thicknesses of CuPc and C_{70}.

The maximum of *G* appears at CuPc(16 nm)/C_{70}(19 nm). So the best structure (thickness combination of donor and acceptor) of the cell is Glass/ ITO(220 nm)/PEDOT:PSS(40 nm)/LiF(1 nm)/CuPc(16 nm)/C_{70}(19 nm)/LiF(1 nm)/Al from the simulation.

Experiments are needed to validate this calculation result. The cells were fabricated in a typical sandwich structure. The ITO-Glass were sequentially cleaned by ultrasonic treatment in acetone, isopropyl alcohol and deionized water, and blown by N_2 gas, and treated by UN-Ozone for 15 min. The UV wavelength used here is 185 nm. The power of the UV lamp is 20 W, which was put in an airtight box with the capacity of about 40 L. Ozone gas was generated by using UV light to excite oxygen in air inside the box. The temperature and humidity inside the box were always kept at 20 ℃ and 30%, respectively.

The purities of CuPc and C_{70} used are 98.5% and 99.9%+, respectively. And they were not further purified before experiments. All the layers in OSCs, expect PEDOT:PSS, were fabricated by vacuum evaporation at a pressure of 2.5×10^{-3} Pa. The thicknesses of the layers were monitored by a quartz oscillator thickness monitor and they were also checked by an ellipsometer. PEDOT:PSS solution (1.3 wt% dispersed in H_2O, conductive grade) was spin-coated on the ITO electrode at 5000 rpm for 30 s, and annealed at 120 ℃ for 15 min. The average thickness of this layer is 40.2 nm measured by an ellipsometer.

The active area of the device is about 0.06 cm^2. The current-voltage characteristics were measured with a Keithley 2400 sourcemeter, under an illumination of 100 mW/cm^2 (monitored by a standard polysilicon solar cell) with an AM1.5G sun simulator.

Since a very accurate thickness control in the experiments was difficult here, 5 nm was used as a thickness step for CuPc and C_{70} layers. The uniformity for an ultrathin film is also a big problem. Thus, the thicknesses of CuPc and C_{70} started from 15 nm.

The short-circuit current density (*Jsc*), open-circuit voltage (*Voc*), calculated fill factor (*FF*), and power conversion efficiency (η) of the fabricated devices are summarized in Table 1. The performances of the cells are not good. This is due to the limitation of equipments. It must break the vacuum and open the equipment cavity to change the evaporation material after finishing depositing a layer. Since much pollution is introduced in the fabrication process, the power conversion efficiencies are several times lower than those reported. But these results still can clearly describe what we want to know.

Table 1. Comparison of characteristics of cells with different CuPc and C_{70} thicknesses.

Structure	Jsc mA/cm^2	Voc mV	FF	η %	Jsc Contrast (Relative Value)	Efficiency Contrast (Relative Value)
CuPc(15 nm)/C_{70}(15 nm)	3.45	596	0.395	0.8122	-4.70%	-6.98%
CuPc(15 nm)/C_{70}(20 nm)	3.62	600	0.402	0.8731	--	--
CuPc(15 nm)/C_{70}(25 nm)	3.73	605	0.407	0.9185	+3.04%	+5.20%
CuPc(15 nm)/C_{70}(30 nm)	3.66	606	0.404	0.8961	+1.10%	+2.63%
CuPc(20 nm)/C_{70}(15 nm)	3.68	599	0.410	0.9038	+1.66%	+3.52%
CuPc(20 nm)/C_{70}(20 nm)	3.72	602	0.412	0.9226	+2.76%	+5.67%
CuPc(20 nm)/C_{70}(25 nm)	3.81	608	0.415	0.9613	+5.25%	+10.10%
CuPc(20 nm)/C_{70}(30 nm)	3.74	612	0.408	0.9339	+3.31%	+6.96%
CuPc(25 nm)/C_{70}(15 nm)	3.58	606	0.408	0.8851	-1.10%	+1.37%
CuPc(25 nm)/C_{70}(20 nm)	3.66	609	0.406	0.9049	+1.10%	+3.64%
CuPc(25 nm)/C_{70}(25 nm)	3.75	612	0.410	0.9410	+3.59%	+7.78%
CuPc(25 nm)/C_{70}(30 nm)	3.69	616	0.402	0.9138	+1.93%	+4.66%

The combination of CuPc(15 nm)/C_{70}(20 nm)in Table 1 is the nearest one to the calculated result. This result is taken as a contrastive base in column Ⅵand Ⅶ of Table 1. But this combination doses not perform very well. The second best combination to the theoretic data is CuPc(20 nm)/C_{70}(20 nm). This cell's performance is much better. When the active layers are very thin, such as CuPc(15 nm)/C_{70}(15 nm), the characteristics of the cell are poor. This agrees with the simulation that the generation rate of effective excitons is low. When the thickness combination is CuPc(25 nm)/C_{70}(15 nm), the Jsc of the cell is also lower than that of the contrastive base (CuPc(15 nm)/C_{70}(20 nm)). This result also agrees with the simulation. However, the efficiency of the cell with CuPc(25 nm)/C_{70}(15 nm) higher than that of the contrastive base cell. The most enhancements are the Voc and FF. From Table 1, the cells' performances are still improving after exceeding the best simulation result, until the thickness combination reaches CuPc(20 nm)/C_{70}(25 nm). It seems that it is good to increase the thickness a little bit from the best calculated result. This problem may come down to the exciton recombination. Eq.(9) only considers the generation of effective excitons. However, actually the recombination also exists. When the thickness is very thin, the effective exciton recombination rate will be a little higher. The interface between the active layer and electrode is one of the most severe recombination areas for excitons. Here the anode interface is taken as an example. Although LiF performs as an anode buffer, there still has a high exciton recombination rate at LiF/CuPc interface. Lots of excitons will be recombined here. The area near LiF/CuPc interface may not be the effective exciton generation region. The density of excitons here is lower because of a high recombination rate. However in the effective exciton generation region inside CuPc layer described above, a higher exciton density exists. So a density gradient is formed between the effective exciton generation region inside CuPc layer and CuPc/LiF interface, like the situation showing in Fig. 7. Many effective excitons will diffuse to the LiF/CuPc interface and will be recombined. This makes the loss of effective excitons. With the increasing of thickness of CuPc layer, the effective exciton generation area can be farther away from LiF/CuPc interface. It makes less influence to the effective excitons and the performances of cells can exhibit better. There a same situation exists for increasing the thickness of C_{70} from 20 nm to 25 nm. So the actual best cell appears at CuPc(20 nm)/C_{70}(25 nm).

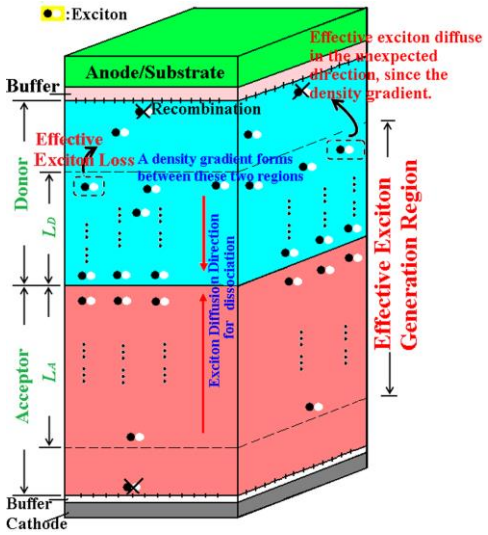

Fig. 7. Sketch map of the loss of effective excitons.

Increasing the thickness can leave the effective exciton generation region far away from the interface of electrodes (including the buffer layers) and decrease the effect of exciton recombination. But if the thickness of donor or acceptor layers continues increasing from the best calculated thickness combination, the effective exciton generation rate is also decreased. Thus, it needs to synthetically consider the rate of generation and recombination in this problem. In Table 1, the actual best thickness combination of layers can be found. From the combination of CuPc(15 nm)/C_{70}(20 nm) to combination of CuPc(20 nm)/C_{70}(25 nm), the decrease of the effective exciton recombination is the main reason for improving cells' performances. With continuing increase of the thickness from CuPc(20 nm)/C_{70}(25 nm) , the decrease of the effective exciton generation rate becomes dominant.

Since the recombination rate of excitons is not considered, there exists a small error between the calculated best thickness combination of donor and acceptor layers from Eq. (9) and the actual results. Fortunately, this error is not so severe, and can be accepted. The rule which the practical thickness combination is a little thicker than that of the calculated data will not change. And this method introduced here provides a search region of thickness combination of donor and acceptor layers for actual experiments.

4. Conclusion

A concept of effective exciton is built in this paper.

Effective exciton generation rate is related to light intensity distribution. Altering the thickness combination of donor and acceptor layers, the light intensity distribution will be also changed. With the effective exciton generation rate maximized, the best thickness

combination will be obtained. This paper gives a calculation method. Photon flux distribution of AM1.5G and transmissivity of substrates have been introduced into the simulation. So this simulation is much closer to practical situation. And using the cell with the structure of Glass/ITO(220 nm)/PEDOT:PSS(40 nm)/LiF(1 nm)/CuPc/C_{70}/LiF(1 nm)/Al(100 nm) as an example, the best combination of donor and acceptor layers is CuPc(16 nm)/C_{70}(19 nm) according to the calculation, and CuPc(20 nm)/C_{70}(25 nm) is the best for actual experiments.

An error of a few nanometers appears between simulation and experiments. This error is caused by the recombination of effective excitons. The recombination rate is not considered in the calculation. A little increasing of the active layers' thickness can leave the effective exciton generation region farther away from the electrode interface, where higher exciton recombination happens.

Although an error exists, it can be accepted. The contribution of this method is to give a search range of thickness combination for donor and acceptor layers.

Moreover, this method can also be used in bulk heterojunction organic solar cells. For a cell with the structure such as Substrate/Anode/Buffer 1/Donor/Bulk Layer/Acceptor/Buffer 2/Cathode, if the refractive indexes and extinction coefficients of all films and all thicknesses except donor and acceptor layers are given, the best thickness combination of donor and acceptor layers also can be calculated from this method. In this case, the effective exciton generation area should include the whole bulk layer, besides the original regions in the simulation model above. In this case, the carrier transportation in the bulk layer might also be additionally considered.

References

[1] N. C. Miller, S. Sweetnam, E. T. Hoke, R. Gysel, C. E. Miller, J. A. Bartelt, X. Xie, M. F. Toney, M. D. McGehee, Nano Letters **12**, 1566 (2012).
[2] F. C. Krebs, J. Fyenbo, M. Jorgensen, Journal Material Chemistry. **20**, 8994 (2010).
[3] M. Jørgensen, O. Hagemann, J. Alstrup, F. C. Krebs, Sol. Energy Mater. Sol. Cells **93**, 413 (2009).
[4] F. C. Krebs, Sol. Energy Mater. Sol. Cells **93**, 465 (2009).
[5] F. C. Krebs, M. Jørgensen, K. Norrman, O. Hagemann, J. Alstrup, T. D. Nielsen, J. Fyenbo, K. Larsen, J. Kristensen, Sol. Energy Mater. Sol. Cells **93**, 422 (2009).
[6] L. Blankenburg, K. Schultheis, H. Schache, S. Sensfuss, M. Schöodner, Sol. Energy Mater. Sol. Cells **93**, 476 (2009).
[7] M. Niggemann, B. Zimmermann, J. Haschke, M. Glatthaar, A. Gombert, Thin Solid Films **516**, 7181 (2008).
[8] F. C. Krebs, H. Spanggard, T. Kjaer, M. Biancardo, J. Alstrup, Mater. Sci. Eng. B **138**, 106 (2007).
[9] C. Lungenschmied, G. Dennler, H. Neugebauer, S. N. Sariciftci, M. Glatthaar, T. Meyer, A. Meyer, Sol. Energy Mater. Sol. Cells **91**, 379 (2007).
[10] C. J. Brabec, Sol. Energy Mater. Sol. Cells **83**, 273 (2004).
[11] G. Yu, J. Gao, J. C. Hummelen, F. Wudl, A. J. Heeger, Science **270**, 1789 (1995).
[12] C. W. Tang, Appl. Phys. Lett. **48**, 183 (1986).
[13] P. Peumans, A. Yakimov, S. R. Forrest, J. Appl. Phys. **93**, 3693 (2003).
[14] J. Ren, J. B. Zheng, J. L. Zhao, Acta Physica Sinica **56**, 2868 (2007).
[15] L. A. A. Petterson, L. S. Roman, O. Inganas, J. Appl. Phys. **86**, 487 (1999).
[16] X. Xi, W. J. Li, J. Q. Wu, J. J. Ji, Z. R. Shi, G. H. Li, Sol. Energy Mater. Sol. Cells **94**, 2435 (2010).
[17] X. Xi, Q. L. Meng, F. X. Li, Y. Q Ding, J. J. Ji, Z. R. Shi, G. H. Li, Sol. Energy Mater. Sol. Cells **94**, 623 (2010).

*Corresponding author: xi_xi_hunt@aliyun.com